Title

Extremely long tumor retention, multi-responsive boronate crosslinked micelles with superior therapeutic efficacy for ovarian cancer

Authors

Xiao, Wenwu

Suby, Nell

Xiao, Kai

et al.

Publication Date

2017-10-01

DOI

10.1016/j.jconrel.2017.08.028

Peer reviewed

HHS Public Access

Author manuscript

J Control Release. Author manuscript; available in PMC 2018 October 28.

Published in final edited form as:

J Control Release. 2017 October 28; 264: 169–179. doi:10.1016/j.jconrel.2017.08.028.

Extremely long tumor retention, multi-responsive boronate crosslinked micelles with superior therapeutic efficacy for ovarian cancer

Wenwu Xiao[1], **Nell Suby**[2], **Kai Xiao**[3], **Tzu-yin Lin**[4], **Nasir Al Awwad**[5], **Kit S. Lam**[1,*], and **Yuanpei Li**[1,*]

[1]Department of Biochemistry and Molecular Medicine, UC Davis Comprehensive Cancer Center, University of California Davis, Sacramento, CA 95817, USA

[2]Division of Gynecologic Oncology, Department of Obstetrics and Gynecology, UC Davis Comprehensive Cancer Center, University of California Davis, Sacramento, CA 95817, USA

[3]National Chengdu Center for Safety Evaluation of Drugs, West China Hospital, Sichuan University, Chengdu, 610041, PR China

[4]Department of Internal Medicine, Division of Hematology/Oncology, University of California Davis, Sacramento, CA 95817, USA

[5]Pathology College of Clinical Pharmacy, Al-Baha University, Al-Baha City, 11074, Saudi Arabia

Abstract

Mortality rates for ovarian cancer have declined only slightly in the past forty years since the “War on Cancer” was declared. The current standard care of ovarian cancer is still cytoredutive surgery followed by several cycles of chemotherapy. The severe adverse effect from chemotherapy drug is a leading cause for the patients to fail in long term therapy post-surgery. New nanocarriers able to minimize the premature drug release in blood circulation while releasing drug on-demand at tumor site have profound impact on the improvement of the efficacy and toxicity profile of the chemotherapeutic drugs. Here we reported a unique type of extremely long tumor retention, multi-responsive boronate crosslinked micelles (BCM) for ovarian cancer therapy. We systemically investigated the stability of BCM in serum and plasma, and their responsiveness to acidic pH and cis-diols (such as mannitol, a safe FDA approved drug for diuresis) through particle size measurement and förster resonance energy transfer (FRET) approach. Paclitaxel (PTX) loaded BCM (BCM-PTX) exhibited higher stability than non-crosslinked micelles (NCM) in the presence of plasma or serum. BCMs possessed a longer *in vivo* blood circulation time when compared to NCM. Furthermore, BCM could be disassembled in an acidic pH environment or by administrating mannitol, facilitating drug release in an acidic tumor environment and triggered by exogenous stimuli after drug enrichment in tumor mass. Near infra-red fluorescence (NIRF) imaging on SKOV-3 ovarian cancer mouse model demonstrated that the NIR dye DiD

*Address correspondence to Yuanpei Li (lypli@ucdavis.edu) or Kit S. Lam (kslam@ucdavis.edu).

encapsulated BCM could preferentially accumulate in tumor site and their tumor retention was very long with still 66% remained on 12th day post injection. DiD-NCM had similar high- level uptake in tumor with DiD-BCM within the first 3 days, its accumulation, however, decreased obviously on 4th day and only 15% dye was left 12 days later. In both formulations, the dye uptake in normal organs was mostly washed away within the first 24–48 hrs. In *in vivo* tumor treatment study, PTX loaded BCM showed superior therapeutic efficacy than that of NCM and Taxol. The mice could tolerate 20 mg/kg PTX formulated in nano-formulations, which doubled the maximum tolerated dose (MTD) of Taxol. The administration of mannitol 24 hrs after BCM-PTX injection further improved the tumor therapeutic effect and elongated the survival time of the mice. The novel boronate-catechol crosslinked nanocarrier platform demonstrated its superior capability in targeted drug delivery, which is not only useful for ovarian cancer treatment but will also be beneficial for the therapy of many other solid tumors.

Graphical abstract

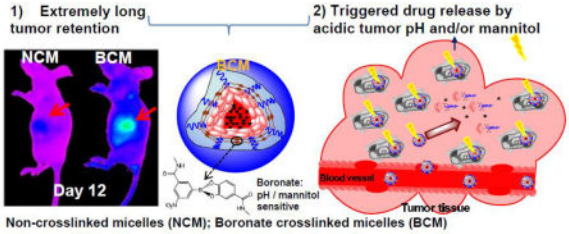

Keywords

Long-term tumor retention; Boronate crosslinked micelles; Multi-responsive; FRET; ovarian cancer

1. Introduction

Ovarian cancer exits as the 5th malignancy resulting in death in female patients. The American Cancer Society estimated that in 2017, about 22,440 new cases of ovarian cancer would be diagnosed and 14,080 women would die of ovarian cancer in the United States[1]. Most epithelial ovarian cancers are diagnosed at an advanced stage where the tumor has seeded the abdominal cavity (stage 3)[2, 3]. The current therapeutic treatments for epithelial ovarian cancers include the use of combination chemotherapy with a platinum based drug and paclitaxel (PTX)[4–9]. If the patient has had an optimal cytoreductive surgery (less than 1cm of residual tumor burden) then the current gold standard of treatment involves intravenous (IV) PTX on Day 1, intraperitoneal (IP) delivery of cisplatin on Day 2, and IP PTX on Day 8, 3 weeks a cycle, repeated a total of 6 cycles. Many patients are unable to complete six cycles due to the debilitating side effects of the chemotherapy. For PTX, these include hypersensitivity reactions, neurotoxicity, and myelosuppression[4–10]. Optimizing drug delivery while decreasing side effects is critical to improve the therapeutic nature of these drugs while also improving a patient's quality of life[11–15].

In the past 10–15 years, nanotechnology has been intensively developed to apply in the field of cancer therapy[12–15]. Polymeric micelles demonstrated their superior potential in drug

delivery for cancer therapy in several aspects, such as superior capability to encapsulate water insoluble chemotherapeutic drugs, prolonged *in vivo* circulation time and preferential accumulation at tumor site via the enhanced permeability and retention (EPR) effect due to their relatively smaller particle size (<100 nm) [11, 16–21]. However, there are some challenges that have hampered the clinical translation of this type of nanoparticles. Polymeric micelles typically are a thermo-dynamic system because they are formed through self-assembled procedure in certain buffer system. It is well-known that a delicate equilibrium exhibits between micelles and unimers in different buffer conditions[22, 23]. Blood is the first biological barrier for micelle-based drug delivery systems via IV administration. It has been demonstrated that the interaction with blood proteins and lipoproteins (e.g. HDL, LDL, VLDL and chylomicron) may cause the dissociation of these thermo-dynamic nanoparticles and lead to premature drug release[24]. Furthermore, conventional polymeric micelles may be dissociated into unimers after IV administration owing to their susceptibility to dilution below the critical micelle concentration (CMC)[22, 23]. This is another factor that may result in early dissociation of the micelles and premature drug release before micelles reaching and accumulating in the tumor location.

Herein, researchers have put more efforts to search for feasible ways to improve the stability of polymeric micelles for *in vivo* drug delivery. Cross- linking approaches have exhibited as one of an ideal choice [25, 26]. A programmable cross-linking strategy to control the release rate of the entrapped drugs in different environments (e.g. normal organs *versus* tumor) is ideal to minimize the systemic toxicity and enhance the therapeutic efficacy of the chemotherapeutic agents. This led to the development of stimuli-responsive cross-linked micelles (SCMs), a smart nanocarrier system for tumor-targeting drug delivery and on demand drug release[19, 23, 27–29]. SCMs possessed minimal premature drug release due to their superior structural stability in blood stream while they could be triggered to release drug payloads in response to the local environment of the tumor (e.g. tumor extra-cellular pH 6.5–7.2 and endosomal/lysosomal pH 4.5–6[30, 31], tumor reductive intra-cellular conditions [19, 23, 26, 32–35], adenosine triphosphate (ATP)[36–38] and enzymes [23]) or exogenous reagents (e.g. N-Acetylcysteine and cis-diols[22, 23, 39]. SCMs have shown great potential to decrease drug accumulation at normal organs to minimize the systemic toxicity and increase the therapeutic index due to their on-demand drug releasing nature at tumor sites.

Boronic acids and cis-diols can form reversible boronate esters, which is responsive dually to external pH value and competing diols[31, 39–48]. Boronate esters have been developed as building blocks in designing stimuli-responsive drug delivery systems. Due to their syn-peri-planar arrangement of the aromatic hydroxy groups and electron-donating character, catechols are an ideal type of diols to form stable boronate ester bond with boronic acids in physiological condition [31]. In the present manuscript, we describe the preclinical development of a unique type of extremely long tumor retention, multi-responsive boronate crosslinked micelles (BCM) for ovarian cancer therapy (Figure1). We utilized förster resonance energy transfer (FRET) approach and particle size measurement to systemically investigate the stability and release profiles of BCM in blood related media such as serum and plasma, and their responsiveness to acidic pH and mannitol. The long-term *in vivo* biodistribution and blood elimination kinetics of BCM were evaluated in SKOV-3 ovarian

cancer mouse models. The therapeutic efficacy and toxicity profiles of BCM entrapped with PTX were further evaluated. To the best of our knowledge, this is the first demonstration of a multi- responsive micelle-based drug delivery system with such long tumor retention (up to 12 days).

2. Materials and method

2.1. Materials

3-Carboxy-5-nitrophenylboronic acid pinacol ester was obtained from Combi-Blocks (San Diego, CA). Monomethylterminated poly ethylene glycol monoamine (MeO-PEG-NH_2, Mw: 5000 Da) was purchased from Rapp Polymere (Tübingen, Germany). PTX was purchased from AK Scientific Inc. (Mountain View, CA). Taxol (Mayne Pharma Paramus, NJ) was obtained from the Comprehensive Cancer Center of University of California, Davis. (Fmoc)lys(Boc)eOH, (Fmoc)Lys(Dde)eOH, (Fmoc)Lys(Fmoc)eOH, and (Fmoc) Ebes-OH were obtained from AnaSpec Inc. (San Jose, CA). 1,1 ’-dioctadecyl-3, 3, 3’, 3’-tetramethylindodicarbocyanine perchlorate (DiD), $DiOC_{18}$ (DiO) and the red-orange dye rhodamine B were purchased from Invitrogen (Carlsbad, CA). Cholic acid and all other chemicals were purchased from Sigma Aldrich (St. Louis, MO).

2.2. Synthesis of telodendrimers

In order to synthesize boronate crosslinked micelles, two distinct building blocks were needed, including telodendrimers containing four 3-Carboxy-5-nitrophenylboronic acid (named as PEG^{5k}-NBA_4-CA_8) and telodendrimers containing four 3,4-Dihydroxybenzoic acids (named as PEG^{5k}-$Catechol_4$-CA_8) (Fig S1)[31]. These telodendrimers were synthesized via solution-phase condensation reactions from MeO-PEG-NH_2 via stepwise peptide chemistry. The PEG^{5k}-CA_8 parent telodendrimer was synthesized to prepare the non-cross-linked micelles according to our previously reported method[11]. To make telodendrimers with fluorescent labeling, rhodamine B isothiocyanate was covalently attached to the amino group of the proximal lysine between PEG and cholic acids in the final telodendrimers[31].

2.3. Preparation of DiD, DiO or PTX loaded micelles

Hydrophobic dye (DiO or DiD) and hydrophobic anti-cancer drug, such as paclitaxel (PTX) were encapsulated into the micelles by the solvent evaporation method as described in our previous studies[22, 31]. Boronate ester bonds formed between boronic acids and catechols of adjacent telodendrimers, upon self-assembly in 1× PBS (All the rest of PBS mentioned are 1× PBS), resulted in the formation of boronate cross-linked micelles (BCM) and drug or dye was encapsulated. Briefly, certain amount of drug or dye, boronic acid-containing telodendrimer and catechol-containing telodendrimer (total 20 mg) were first dissolved in anhydrous chloroform in a 10 mL round bottom flask. The chloroform was evaporated under vacuum to form a thin film. PBS buffer (1 mL) was added to re-hydrate the thin film, followed by 30 min of sonication. The unloaded PTX or dye was removed by running the micelle solutions through centrifugal filter devices (MWCO: 3.5 kDa, Microcon®). The PTX or dye loaded micelles on the filters were recovered with PBS.

The amount of drug loaded in the micelles was analyzed on a HPLC system (Waters) equipped with a diode array UV detector after releasing the drugs from the micelles by adding 9 times of acetonitrile and 10 min sonication. The mobile phase consisted of a mixture of water and acetonitrile (50:50, v/v%). C18 analytical column (150 mm 4.6 mm, 5 μm, Waters) was employed to separate the samples, and the flow speed was set to 1 mL/min. The whole eluting procedure lasted for 10 min. The calibration curve of PTX was obtained using a series of drug/DMSO standard solutions with different concentrations. The drug loading was calculated according to the calibration curve between the HPLC area va lues and concentrations of standard. The loading efficiency is defined as the ratio of drug loaded into micelles to the initial drug content. The amount of dye loaded in the micelles was analyzed on a fluorescence spectrometry (SpectraMax M2, Molecular Devices, USA) after releasing the drugs from the micelles by adding 9 times of acetonitrile and 10 min sonication. The dye loading was calculated according to the calibration curve between the fluorescence intensity and concentrations of dye standard in acetonitrile. The final micelle solution was filtered with 0.22 μm filter to sterilize the sample.

2.4. Characterizations of micelles

The size and size distribution of the micelles were measured by dynamic light scattering (DLS) instruments (Microtrac). The micelle concentrations were kept at 1.0 mg/mL for DLS measurements. Each sample was measured for three times with an acquisition time of 30 seconds at room temperature. The data were analyzed by Microtrac FLEX Software 10.5.3 and values were reported as the means for each triplicate measurements. The morphology of micelles was observed on a Philips CM-120 transmission electron microscope (TEM). The aqueous micelle solution (1.0 mg/mL) was deposited onto copper grids, stained with phosphotungstic acid, and measured at room temperature.

2.5. Stability investigations of PTX loaded micelles in SDS and human plasma

To investigate the stability of PTX loaded micelles, the change in particle size of NCM and BCM after encapsulation of PTX was monitored in the presence of sodium dodecyl sulfate (SDS), which was reported to be able to efficiently break down polymeric micelles [22, 23]. The final concentration of micelles was kept at 1.0 mg/mL while that of SDS was 2.5 mg/mL. The size and size distribution of the micelle solutions was monitored continuously via DLS instruments for 2 days. The stability of the micelles was also evaluated in PBS at different pH levels or in presence of mannitol and glucose (0, 10 mM, 50 mM, and 100 mM), together with SDS. Hydrogen chloride and sodium hydroxide solutions were used to prepare PBS at different pH levels. The pH values of the buffer were determined by a digital pH meter (Φ350 pH/Temp/mV meter, Beckman Coulter, USA) which gave pH values within 0.01 units. During the stability study, a small portion of the samples were taken out and further observed under TEM. The stability of NCM and BCM was further studied in 50% (v/v) plasma from healthy human volunteers. The mixture was incubated at physiological body temperature (37 °C) followed by size measurements at predetermined time intervals up to 96 hrs.

2.6. In vitro FRET studies

PEG^{5k}-CA$_8$ (15 mg), rhodamine B conjugated PEG^{5k}-CA$_8$ (5 mg) and DiO (0.5 mg) were used to prepare non-crosslinked FRET micelles (FRET-NCM) based on the methods described in Section 2.5 while PEG^{5k}-BA$_4$-CA$_8$(5 mg), rhodamine B conjugated PEG^{5k}-NBA$_4$-CA$_8$ (5 mg), PEG^{5k}-Catechol$_4$-CA$_8$ (10 mg) and DiO (0.5 mg) were used to prepare crosslinked FRET micelles (FRET-BCM). Micelles with DiO alone and micelles with rhodamine B alone at the same dye contents were also prepared for comparison. The micelle solution was filtered with 0.22 μm filter to sterilize the sample. The absorbance and fluorescence spectra of these micelles diluted by PBS were characterized by fluorescence spectrometry (SpectraMax M2, Molecular Devices, USA). The excitation was set to 480 nm while the emission was recorded from 500 nm to 660 nm. The FRET ratio was calculated by the formula of ($I_{rhodamine\ B}$/($I_{rhodamine\ B}$ + I_{DiO})), where $I_{rhodamine\ B}$ and I_{DiO} were fluorescence intensity of rhodamine B at 580 nm and DiO at 530 nm, respectively. The FRET signal changes were evaluated in PBS as well as in fetal bovine serum (FBS) at different pH levels or in presence of mannitol and glucose.

2.7. Animal and tumor xenograft model

Female athymic nude mice (Nu/Nu strain), 6–8 weeks age, were purchased from Harlan (Livermore, CA). All animals were kept under pathogen- free conditions according to AAALAC guidelines and were allowed to acclimatize for at least 4 days prior to any experiments. All animal experiments were performed in compliance with institutional guidelines and according to protocols approved by the Animal Use and Care Administrative Advisory Committee at the University of California, Davis. The subcutaneous xenograft model of ovarian cancer was established by injecting 5×10^6 SKOV-3 ovarian cells in a 100 μL of PBS subcutaneously into the right flank of female nude mice.

2.8. In vivo blood elimination kinetics and long-term biodistribution

To compare the pharmacokinetics of NCM and BCM, we injected 100 μL of DiD (0.5mg/mL) loaded micelles (20 mg/mL) into nude mice bearing SKOV-3 avian cancer xenografts *via* tail vein. At pre-determined time points, 50 μL of blood were collected and DiD fluorescence signal in the serum were measured using fluorescence spectrometry (SpectraMax M2, Molecular Devices, USA). For long-term biodistribution study, nude mice with established subcutaneous SKOV-3 xenograft tumors (8–10 mm in diameter) were subjected to *in vivo* NIRF optical imaging. After injected 100 μL of DiD and PTX co-loaded BCM (0.5 mg/mL of DiD; 0.5 mg/mL of PTX), whole mouse NIRF imaging were acquired under general anesthesia at different time points on a Kodak multimodal imaging system IS2000MM with an excitation bandpass filter at 625 nm and an emission at 700 nm. At each time point, mice were sacrificed and all major organs and tumors were harvested for acquiring *ex vivo* NIRF imaging.

2.9. In vivo therapeutic and toxicity studies

Anti-cancer efficacy study was performed on SKOV-3 xenograft mouse model. Briefly, after the tumors reached a volume of 100–200 mm^3, mice were randomized into eight groups (PBS, 10 mg/kg Taxol, 10 mg/kg NCM-PTX, 20 mg/kg NCM-PTX, 10 mg/kg BCM-PTX,

20 mg/kg BCM-PTX, 10 mg/kg BCM-PTX plus 200 uL 20% mannitol, and 20mg/kg BCM-PTX plus 200 uL 20% mannitol). Drugs were given twice a week for a total of 7 doses. Tumor size (formula used: (Length×Width^2)/2 mm^3), and body weight were monitored twice a week and mice were monitored daily for its appearance, hair coat, behavior, and spirits. Of note, 10 mg/kg Taxol was chosen as it was close to its maximum tolerated dose (MTD) [11, 49]. We previously showed that the MTD for NCM-PTX formulation could reach 75mg/kg [11]. Therefore, we included the 20 mg/kg as a higher dose level for both BCM-PTX and NCM-PTX groups to evaluate if the anti-cancer efficacy could be further improved. Mannitol solutions were IV administered 24 hrs post- injection and were used to trigger drug release from BCM-PTX in tumor site. When tumor size reached 1500 mm^3, for humane reasons, animals were terminated. Animal survival data were recorded till day 82. To monitor potential toxicity, the body weight of each mouse was measured every 3 days. At day 6 after the last dose, blood samples were collected from each group to test blood cell counts and serum chemistry.

2.10. Statistical analysis

Statistical analysis was performed by Student's t-test for two groups, and oneway ANOVA for multiple groups. All results were expressed as the mean ± standard error (mean ± SEM) unless otherwise noted. A value of $P < 0.05$ was considered statistically significant.

3. Results and discussion

3.1. Characterizations of PTX-loaded BCMs

BCM were formed by the self-assembly of two distinct telodendrimers: boronic acid-containing telodendrimer (PEG^{5k}-NBA$_4$-CA$_8$) and catechol-containing telodendrimers (PEG^{5k}-Catechol$_4$-CA$_8$) (FigS1). Upon the self-assembly of PEG^{5k}-NBA$_4$-CA$_8$ and PEG^{5k}-Catechol$_4$-CA$_8$ in PBS, *in situ* crosslinkages were formed by boronate ester bonds between boronic acids and catechols of adjacent telodendrimers, result ing in the formation of boronate cross- linked micelles (BCM) (Fig1) [31]. Nitro-phenylboronic acid was chosen over phenylboronic acid because pKa of nitro-phenylboronic acid is lower (6.9) [31, 48] and therefore the resulting crosslinkage is expected to be more stable at physiological pH of the blood. A wide-spectrum anti-tumor agent, PTX, could be successfully encapsulated into the hydrophobic interior of BCMs simultaneously. At an initial PTX level at 2.0 mg/mL, the drug loading was almost 2.0 mg/mL while the entrapment efficiencies were 100 ± 5%. The final particle sizes of PTX- loaded BCMs (BCM-PTX) were in the range of 20–30 nm as observed under TEM (Fig2). The morphology of these PTX loaded BCMs was observed to be spherical (Fig. 2). The size of the micelles observed under TEM were consistent with those measured by DLS (Fig. 3D).

3.2. The particle size of PTX-BCMs under different conditions

The intra-micellar boronate ester crosslinkages of BCM-PTX greatly enhanced their stability in physiological conditions in human plasma as well as severe micelle-disrupting conditions with neutral pH. DLS instrument was used to measure the size and size distribution of BCM-PTX, from which the stability of micelles could be evaluated. The stability of PTX loaded non-crosslinked micelles (NCM-PTX) and BCM-PTX were investigated in the presence of

plasma, SDS, adjusted pH and mannitol. The average particle size of NCM-PTX increased in the presence of plasma and the size distribution became much broader, indicating the formation of big aggregations upon interaction with blood proteins (Table1, Fig 3A and B). In contrast, the size of BCM-PTX with the presence of plasma was almost the same with that in the absence of plasma (Fig 3D and E). The NCM-PTX disassembled shortly after treated with SDS (Fig 3C). However, BCM-PTX still kept intact in SDS (Fig 3F) with pH 7.4, only dissociating when pH was adjusted to 5.0 (Fig 3G) or when mannitol (Fig 3H) was supplemented in the solution. The addition of glucose did not show similar effect as that of mannitol (Fig 3I). Collectively, the BCM-PTX was stable in normal plasma, in glucose solution and in physiologic pH with the presence of strong micelle-disrupting agents SDS, which implied that the nanomicelle was able to keep integrity in normal blood system, therefore could circulate for longer time. In addition, the BCM-PTX could be dissociated when they were treated with acidic condition or mannitol, which meant that the loaded PTX could be released in a controllable manner. Mannitol is a safe FDA approved drug for diuresis. A high blood level of mannitol (>50 mM) can be achieved clinically based on the recommended dose. Mannitol can thus be applied *in vivo* as an on-demand cleavage reagent by systemic IV injection to trigger drug release after the drug- loaded BCM have accumulated in tumor sites. The above results generally indicated that BCM-PTX possessed superior stability in the presence of plasma compared to NCM-PTX. Furthermore, BCM-PTX could disassemble in an acidic environment (intratumor or lysosome) or in the presence of mannitol, which is an important feature for the intra-tumor or on-demand drug release.

3.3. pH- and sugar- response of boronate crosslinked micelles detected by FRET

FRET is a physical phenomenon first described over 50 years ago. FRET relies on the distance-dependent transfer of energy from a donor molecule to an acceptor molecule. FRET is a powerful technique to probe the molecular proximity of a fluorescent donor-acceptor pair and has been widely applied in the investigation of a variety of biological molecular interaction[50, 51]. Recently, FRET technique has been utilized to probe the stability and drug release profile of micelles[24, 52, 53]. In this paper, we developed a FRET system to further evaluate the stability and drug release of our boronate-crosslinked micelles in serum and/or in the presence of acidic pH and mannitol. We constructed the FRET pair with a green dye DiO (donor) and a red-orange dye rhodamine B (acceptor)(Fig 4, Fig S2, S3). DiO was encapsulated in the core of micelles as the hydrophobic drug surrogate to track the payloads. Rhodamine B was covalently conjugated to the telodendrimers to track the nanocarriers. Both FRET-NCM[24] and FRET-BCM were very stable in PBS at pH7.4, thus there was little change in FRET signal over time (Fig S3). However, a dramatic decrease in FRET signal for FRET-NCM was observed within 30 min in the presence of fetal bovine serum (FBS) (Fig 4A), probably due to the interaction of micelles with blood proteins and lipoprotein nanoparticles (e.g. LDL, HDL, VLDL) in FBS. The FRET ratio decreased to 29% at 6 hrs (Fig 5 **cyan line**). On the contrary, there was much less change in the FRET signal for FRET-BCM up to 24 h in the present of FBS (Fig 4B, Fig 5, **black line**). The boronate crosslinking significantly increased the stability of micelles, preventing the interactions of micelles with blood proteins in FBS, therefore minimizing the drop of FRET signal.

The response of BCM to pH and mannitol was studied by detecting the change in FRET signal over time in FBS. There was a significant decrease of FRET signal when mannitol or acidic pH 5.0 were present respectively (Fig S4A & B, Fig5 **red line & green line**) compared to that in FBS only (Fig 4B, Fig 5, **black line**). The most dramatic decrease of FRET signal of BCM could be observed when mannitol and acidic pH 5.0 were present concurrently (Fig5 **blue line,** Fig 6). The rapid decrease from 89% to 38% in FRET signal was observed within the initial 1.5 hrs (Fig5 **blue line**). As a control, high concentration of glucose (100 mM) only had minimal affect on the FRET signal of BCMs (Fig5 **purple line**). The results from FRET studies further demonstrated that BCM possessed significantly enhanced *in vitro* stability and was ready to disintegrate and release the payload in the presence of acidic pH and/or mannitol, which was in agreement with the results from the size measurement under various conditions.

3.4. In vivo blood elimination kinetics

To explore and compare the effects of boronate ester crosslinked nanoparticles on drug elimination in blood stream of live animals, we loaded a hydrophobic NIRF dye, DiD, into BCM serving as a drug surrogate. We compared the *in vivo* blood elimination kinetics DiD loaded BCM with DiD loaded NCM. As shown in Fig S5 A&B, we first confirmed that the loading level of DiD was equivalent in BCM and NCM based on the absorbance and fluorescence analysis. DiD loaded BCM and NCM were injected via tail vein into nude mice bearing SKOV-3 ovarian cancer, blood was collected at different time points up to 32 hrs (Fig 7). The serum fluorescence intensity peaked at 1.5 and 4 hrs post- injections of NCM and BCM, respectively. In contrast to NCM formulation, fluorescence from BCM formulation was still detectable even at 32 hrs after injection. Most importantly, BCM exhibited significantly greater area under curve (AUC) compared to NCM (Fig 7). Consistent with previous *in vitro* stability studies, these results strongly support the conclusion that BCM exhibited better *in vivo* stability than NCM. It should be noted that the peak values in the curve of BCM and NCM were reached at 4 hrs and 1.5 hrs after injection, respectively, but not at the very beginning. By comparing the fluorescence intensity in PBS and DMSO, we observed fluorescence quenching in both DID loaded NCM and BCM (Figure S5B). With gradual dissociation of the nanoparticles, more and more DiD dye without signal quenched was released into blood stream to induce a lagged peak.

3.5. Prolonged retention of DiD-loaded BCM in ovarian cancer xenografts

To evaluate and compare the tumor targeting efficiency of BCM and NCM, DiD and PTX co- loaded BCM and NCM were administrated into nude mice bearing SKOV-3 ovarian cancer xenograft intravenously and the *in vivo* and *ex vivo* optical imaging were performed at pre-determined time points up to 12 days post- injection. Both DiD-PTX BCM and DiD-PTX NCM showed obvious tumor accumulation and reached peaks at around 24 hrs post-injection (Fig 8A&B), but their accumulation decreased at different rate (Fig 8&9). The uptake of both nano- formulations in tumor maintained at a high level within first 3 days. The uptake plateau for DiD-PTX BCM lasted to 7^{th} day while the accumulation for DiD-PTX NCM showed obvious decrease starting from the 4^{th} day. On 12^{th} day after injection, there was 66% of DiD-PTX-BCM still kept in tumor but only 15% remained for DiD-PTX NCM (Fig 9). In general, both BCM and NCM were able to deliver DiD and PTX into

tumor, but BCM showed longer tumor retention. It was noted that in both nano-formulations there were moderate degrees of liver, lung and interstine accumulation of DiD fluorescence signal in the early time-points, but that nonspecific accumulation degraded quickly (eliminated from the body) while tumors remained with high amount of NIRF signals (Fig 9). The off- target uptake in normal organs such as liver or lung is a common phenomenon for nanoparticles. Our group had reported that slightly negative charge could be introduced to the nanoparticles surface to reduce the undesirable clearance by the reticuloendothe lial system (RES) such as liver[54], which was one of ways beneficial to reducing nonspecific uptake in normal organs.

Collectively, these results demonstrated that, compared with NCM, BCM was able to more specifically and efficiently deliver their payload to ovarian cancer xenograft and remain at a higher concentration in the tumor for a long time (at least 12 days). This result has great therapeutic implication as it illustrated that payload inside the boronate crosslinked nanoparticles could retain in the tumor site for multiple days, thus allowing sustained *in situ* therapy to the tumor while sparing normal organs. This tumor selective and long-term retention effect allows sustained anti-cancer effects and decreased toxicity toward normal organs.

3.6. Therapeutic efficacies of PTX-loaded BCM

The standard treatment for ovarian cancer was mentioned above. After optimal tumor debulking, PTX (IV) at day 1, Cisplatin (IP) at day 2 and PTX (IP) at day 8 are sequentially applied every 3 weeks for total 6 cycles. A big issue for the chemotherapy is the patients could not tolerate the severe side effects such as hypersensitivity reactions, neurotoxicity, and myelosuppression etc[10, 55–57]. Here we investigated that whether BCM with encapsulated chemotherapeutic agents could facilitate improved drug delivery to the tumor environment for enhanced therapeutic efficacy, and reduced the systemic toxicity. We evaluated the therapeutic efficacy of BCM-PTX on nude mice bearing SKOV-3 tumor xenograft with the groups and treatments indicated in Fig 10. Mice were treated twice a week with a total dose of 7. It was important to note that SKOV-3 tumor xenograft in this experiment appeared to be resistant to the Taxol therapy. Nevertheless, both BCM-PTX and NCM-PTX exhibited significantly superior anti-cancer efficacy and prolonged survival compared to free Taxol at 10 mg/kg ($p<0.05$) (Fig 10 A&B). Specifically, the medium survival times for 10 mg/kg Taxol, NCM-PTX and BCM-PTX were 27.5, 34, and 43 days, respectively. The therapeutic efficacy was improved even further when mice were treated with mannitol at 24 hrs after the injection of BCM-PTX for triggering the drug release on-demand when these nanoparticle drugs accumulated at the tumor sites (Fig 10 A&B). This treatment could significantly prolong the medium survival days to 51.5 days. In this study, we also treated animals with both PTX nano-formulations (NCM-PTX and BCM-PTX) at 20 mg/kg (double the MTD dose of Taxol) to see if we could further enhance anti-cancer efficacy. We found that all mice were able to tolerate this dose level (20 mg/kg) without obvious body weight loss. At this high dose (20 mg/kg), all tumors shrank 50–70% (NCM-PTX: 54%, DCM-PTX: 70%, DCM-PTX plus mannitol: 74%) and some of them even achieved complete remission. Although some tumors appeared to regrow after day 50, BCM-PTX was significantly more efficacious than NCM-PTX at 20 mg/kg, while BCM-

PTX with mannitol further advanced the anti-cancer efficacy (Fig 10 A&B). The medium survival time for 20 mg/kg NCM-PTX, BCM-PTX, and BCM-PTX plus mannitol were 72, 81, and >82 days, respectively. The complete tumor response rate of 33% was achieved with the combination treatment of BCM-PTX and mannitol. In contrast, the complete tumor response rate is only 10% for the same treatment group without manntiol.

Systemic toxicity was first monitored based on the body weight change and no significant body weight loss was noted in all groups. We further collected blood 6 days post last treatment and analyzed complete blood count (CBC) and serum chemistry for liver/kidney functions. As shown in Table S1 and S2, no obvious toxicity was noted and all values were within the normal range. These results suggested that even with the administration of BCM-PTX at the level equivalent to twice of the MTD doses of free drug, mice could still tolerate and no significantly increased toxicity was observed.

Collectively, BCM-PTX exhibited superior therapeutic efficacy likely attributed to the prolonged drug circulation time and extremely long retention at the tumor site. The administration of mannitol with BCM-PTX could further trigger the drug release at the tumor sites and thus further enhanced the therapeutic index. Similar to NCM formulation, BCM could be given at least two folds of the MTD dose of Taxol without increased toxicity. In the other words, mice or patients could receive higher doses of chemotherapy with our novel formulation and achieve remarkable outcome without suffering from additional toxicity. It is expected that decoration of cancer cell-specific ligands on the surface of BCM would offer better delivery of even higher drug dose into tumor to achieve further enhanced therapeutic efficacy[18].

It is necessary to note that, compared with BCM, NCM did show less stability and shorter circulation time. But from the *in vivo* biodistribution and therapeutic experiments, NCM also demonstrated its potential to deliver DiD and PTX to tumor location, attributed to the common EPR effect of nanoparticles. Our groups had reported that drug loaded NCM was efficacious in several tumor models as well [11, 20]. Therefore, it is not surprising that PTX-NCM indicated obvious *in vivo* therapeutic effect in this research. PTX-BCM demonstrated its significantly improved therapeutic effect as a result of enhanced stability in 10mg/kg and 20mg/kg groups. But the improved effect in group 20mg/kg was not as great as in that of 10mg/kg. This is likely caused by that the 7 doses of drug were administrated within first three weeks, and by the time of 6 or 7 weeks after last dose, most the drug might be washed away. An alternative way to amply the difference is to increase the number of dosing or give the supplementary dose after 6–7 weeks, which would be tested in our future experiments.

4. Conclusion

To improve the efficacy of chemotherapy against ovarian cancer and reduce systemic side effect from the drug, we developed an unique catechol-boronate crosslinked micellar drug delivery system. BCM demonstrated superior *in vitro* stability in the presence of plasma under physiological pH, but dissociated when treated with acidic pH and/or mannitol, but not with glucose. BCM also showed higher *in vivo* stability compared with their non-crosslinked counterpart. BCM possessed extremely long tumor retention time up to 12 days

after injection in mice. After loading with PTX, BCM were demonstrated to have better therapeutic effect against SKOV-3 ovarian cancer in mouse model in contrast to that of NCM and Taxol. Furthermore, the therapeutic efficacy of BCM-PTX could be further enhanced by the administration of mannitol for triggering drug release at the tumor site on-demand. This triggering release mechanism can also be expanded to other stimuli- responsive drug delivery systems. This important observation has great translational potential and can be easily tested in clinical trials in the future as mannitol is already used in clinic at high dose. The extremely long tumor retention, multi-responsive crosslinked nano-platform shows great promise to improve the efficacy and minimize the side effect of the treatment for ovarian cancer. It could be potentially utilized to treat many other tumor types beside ovarian cancer after loading with corresponding chemotherapy drugs.

Supplementary Material

Refer to Web version on PubMed Central for supplementary material.

Acknowledgments

The authors thank the financial support from NIH/NCI (R01CA199668 & 3R01CA115483), NIH/NIBIB (5R01EB012569), NIH/NICHD (1R01HD086195) and DoD PRMRP Award (W81XWH-13-1-0490).

References

1. Siegel RL, Miller KD, Jemal A. Cancer Statistics, 2017. CA Cancer J Clin. 2017; 67:7–30. [PubMed: 28055103]
2. Matz M, Coleman MP, Carreira H, Salmeron D, Chirlaque MD, Allemani C. Worldwide comparison of ovarian cancer survival: Histological group and stage at diagnosis (CONCORD-2). Gynecologic oncology. 2017; 144:396–404. [PubMed: 27919574]
3. Corzo C, Iniesta MD, Patrono MG, Lu KH, Ramirez PT. Role of Fallopian Tubes in the Development of Ovarian Cancer. Journal of minimally invasive gynecology. 2017; 24:230–234. [PubMed: 28007588]
4. Bergamini A, Ferrero S, Leone Roberti Maggiore U, Scala C, Pella F, Vellone VG, Petrone M, Rabaiotti E, Cioffi R, Candiani M, Mangili G. Folate receptor alpha antagonists in preclinical and early stage clinical development for the treatment of epithelial ovarian cancer. Expert opinion on investigational drugs. 2016; 25:1405–1412. [PubMed: 27797594]
5. Suh DH, Kim M, Kim HJ, Lee KH, Kim JW. Major clinical research advances in gynecologic cancer in 2015. Journal of gynecologic oncology. 2016; 27:e53. [PubMed: 27775259]
6. Hellner K, Miranda F, Fotso Chedom D, Herrero-Gonzalez S, Hayden DM, Tearle R, Artibani M, KaramiNejadRanjbar M, Williams R, Gaitskell K, Elorbany S, Xu R, Laios A, Buiga P, Ahmed K, Dhar S, Zhang RY, Campo L, Myers KA, Lozano M, Ruiz-Miro M, Gatius S, Mota A, Moreno-Bueno G, Matias-Guiu X, Benitez J, Witty L, McVean G, Leedham S, Tomlinson I, Drmanac R, Cazier JB, Klein R, Dunne K, Bast RC Jr, Kennedy SH, Hassan B, Lise S, Garcia MJ, Peters BA, Yau C, Sauka-Spengler T, Ahmed AA. Premalignant SOX2 overexpression in the fallopian tubes of ovarian cancer patients: Discovery and validation studies. EBioMedicine. 2016; 10:137–149. [PubMed: 27492892]
7. Ramalingam P. Morphologic, Immunophenotypic, and Molecular Features of Epithelial Ovarian Cancer. Oncology (Williston Park). 2016; 30:166–176. [PubMed: 26892153]
8. Park CS, Kim TK, Kim HG, Kim YJ, Jeoung MH, Lee WR, Go NK, Heo K, Lee S. Therapeutic targeting of tetraspanin8 in epithelial ovarian cancer invasion and metastasis. Oncogene. 2016; 35:4540–4548. [PubMed: 26804173]

9. Fagotti A, Perelli F, Pedone L, Scambia G. Current Recommendations for Minimally Invasive Surgical Staging in Ovarian Cancer. Current treatment options in oncology. 2016; 17:3. [PubMed: 26739150]
10. Rooth C. Ovarian cancer: risk factors, treatment and management. Br J Nurs. 2013; 22:S23–30.
11. Xiao K, Luo J, Fowler WL, Li Y, Lee JS, Xing L, Cheng RH, Wang L, Lam KS. A self-assembling nanoparticle for paclitaxel delivery in ovarian cancer. Biomaterials. 2009; 30:6006–6016. [PubMed: 19660809]
12. Zeineldin R, Syoufjy J. Cancer Nanotechnology: Opportunities for Prevention, Diagnosis, and Therapy. Methods in molecular biology. 2017; 1530:3–12. [PubMed: 28150193]
13. Gmeiner WH, Ghosh S. Nanotechnology for cancer treatment. Nanotechnology reviews. 2015; 3:111–122. [PubMed: 26082884]
14. Goldberg MS. Immunoengineering: how nanotechnology can enhance cancer immunotherapy. Cell. 2015; 161:201–204. [PubMed: 25860604]
15. Grodzinski P, Farrell D. Future opportunities in cancer nanotechnology--NCI strategic workshop report. Cancer research. 2014; 74:1307–1310. [PubMed: 24413533]
16. Kern HB, Srinivasan S, Convertine AJ, Hockenbery D, Press OW, Stayton PS. Enzyme-Cleavable Polymeric Micelles for the Intracellular De-livery of Pro-Apoptotic Peptides. Mol Pharm. 2017
17. Wang Q, Jiang H, Li Y, Chen W, Li H, Peng K, Zhang Z, Sun X. Targeting NF-kB signaling with polymeric hybrid micelles that co-deliver siRNA and dexamethasone for arthritis therapy. Biomaterials. 2017; 122:10–22. [PubMed: 28107661]
18. Xiao K, Li Y, Lee JS, Gonik AM, Dong T, Fung G, Sanchez E, Xing L, Cheng HR, Luo J, Lam KS. "OA02" peptide facilitates the precise targeting of paclitaxel- loaded micellar nanoparticles to ovarian cancer in vivo. Cancer research. 2012; 72:2100–2110. [PubMed: 22396491]
19. Xiao K, Li YP, Wang C, Ahmad S, Vu M, Kuma K, Cheng YQ, Lam KS. Disulfide cross-linked micelles of novel HDAC inhibitor thailandepsin A for the treatment of breast cancer. Biomaterials. 2015; 67:183–193. [PubMed: 26218744]
20. Xiao K, Luo J, Li Y, Lee JS, Fung G, Lam KS. PEG-oligocholic acid telodendrimer micelles for the targeted delivery of doxorubicin to B-cell lymphoma. Journal of Controlled Release. 2011
21. Li Y, Xiao K, Luo J, Lee J, Pan S, Lam KS. A novel size-tunable nanocarrier system for targeted anticancer drug delivery. Journal of Controlled Release. 2010; 144:314–323. [PubMed: 20211210]
22. Li Y, Xiao K, Luo J, Xiao W, Lee JS, Gonik AM, Kato J, Dong TA, Lam KS. Well-defined, reversible disulfide cross-linked micelles for on-demand paclitaxel delivery. Biomaterials. 2011; 32:6633–6645. [PubMed: 21658763]
23. Li Y, Xiao K, Zhu W, Deng W, Lam KS. Stimuli-responsive cross-linked micelles for on-demand drug delivery against cancers. Adv Drug Deliv Rev. 2014; 66:58–73. [PubMed: 24060922]
24. Li Y, Budamagunta MS, Luo J, Xiao W, Voss JC, Lam KS. Probing of the assembly structure and dynamics within nanoparticles during interaction with blood proteins. ACS nano. 2012; 6:9485–9495. [PubMed: 23106540]
25. Thurmond KB, Kowalewski T, Wooley KL. Water-soluble knedel-like structures: The preparation of shell-cross-linked small particles. Journal of the American Chemical Society. 1996; 118:7239–7240.
26. Kakizawa Y, Harada A, Kataoka K. Environment-sensitive stabilization of core-shell structured polyion complex micelle by reversible cross-linking of the core through disulfide bond. Journal of the American Chemical Society. 1999; 121:11247–11248.
27. Xin K, Li M, Lu D, Meng X, Deng J, Kong D, Ding D, Wang Z, Zhao Y. Bioinspired Coordination Micelles Integrating High Stability, Triggered Cargo Release, and Magnetic Resonance Imaging. ACS applied materials & interfaces. 2017; 9:80–91. [PubMed: 27957858]
28. Mittal A, Chitkara D. Structural modifications in polymeric micelles to impart multifunctionality for improved drug delivery. Therapeutic delivery. 2016; 7:73–87. [PubMed: 26769002]
29. Rodriguez-Hernandez J, Babin J, Zappone B, Lecommandoux S. Preparation of shell cross-linked nano-objects from hybrid-peptide block copolymers. Biomacromolecules. 2005; 6:2213–2220. [PubMed: 16004465]

30. Li Z, Wang H, Chen Y, Wang Y, Li H, Han H, Chen T, Jin Q, Ji J. pH- and NIR Light-Responsive Polymeric Prodrug Micelles for Hyperthermia-Assisted Site-Specific Chemotherapy to Reverse Drug Resistance in Cancer Treatment. Small. 2016; 12:2731–2740. [PubMed: 27043935]
31. Li Y, Xiao W, Xiao K, Berti L, Luo J, Tseng HP, Fung G, Lam KS. Well-defined, reversible boronate crosslinked nanocarriers for targeted drug delivery in response to acidic pH values and cis-diols. Angew Chem Int Ed Engl. 2012; 51:2864–2869. [PubMed: 22253091]
32. Koo AN, Lee HJ, Kim SE, Chang JH, Park C, Kim C, Park JH, Lee SC. Disulfide-cross-linked PEG-poly(amino acid)s copolymer micelles for glutathione-mediated intracellular drug delivery. Chemical Communications. 2008:6570–6572. [PubMed: 19057782]
33. Li YL, Zhu L, Liu ZZ, Cheng R, Meng FH, Cui JH, Ji SJ, Zhong ZY. Reversibly Stabilized Multifunctional Dextran Nanoparticles Efficiently Deliver Doxorubicin into the Nuclei of Cancer Cells. Angewandte Chemie-International Edition. 2009; 48:9914–9918. [PubMed: 19937876]
34. Miyata K, Kakizawa Y, Nishiyama N, Harada A, Yamasaki Y, Koyama H, Kataoka K. Block catiomer polyplexes with regulated densities of charge and disulfide cross-linking directed to enhance gene expression. J Am Chem Soc. 2004; 126:2355–2361. [PubMed: 14982439]
35. Wang YC, Li Y, Sun TM, Xiong MH, Wu JA, Yang YY, Wang J. Core-Shell-Corona Micelle Stabilized by Reversible Cross-Linkage for Intracellular Drug Delivery. Macromolecular rapid communications. 2010; 31:1201–1206. [PubMed: 21590876]
36. Qian C, Chen Y, Zhu S, Yu J, Zhang L, Feng P, Tang X, Hu Q, Sun W, Lu Y, Xiao X, Shen QD, Gu Z. ATP-Responsive and Near-Infrared-Emissive Nanocarriers for Anticancer Drug Delivery and Real-Time Imaging. Theranostics. 2016; 6:1053–1064. [PubMed: 27217838]
37. Sun W, Gu Z. ATP-Responsive Drug Delivery Systems. Expert opinion on drug delivery. 2016; 13:311–314. [PubMed: 26745457]
38. Mo R, Jiang T, DiSanto R, Tai W, Gu Z. ATP-triggered anticancer drug delivery. Nat Commun. 2014; 5:3364. [PubMed: 24618921]
39. Ma R, Yang H, Li Z, Liu G, Sun X, Liu X, An Y, Shi L. Phenylboronic acid-based complex micelles with enhanced glucose-responsiveness at physiological pH by complexation with glycopolymer. Biomacromolecules. 2012; 13:3409–3417. [PubMed: 22957842]
40. Qu Q, Wang Y, Zhang L, Zhang X, Zhou S. A Nanoplatform with Precise Control over Release of Cargo for Enhanced Cancer Therapy. Small. 2016; 12:1378–1390. [PubMed: 26763197]
41. Zhang R, Su S, Hu K, Shao L, Deng X, Sheng W, Wu Y. Smart micelle@polydopamine core-shell nanoparticles for highly effective chemo-photothermal combination therapy. Nanoscale. 2015; 7:19722–19731. [PubMed: 26556382]
42. Matuszewska A, Uchman M, Adamczyk-Wozniak A, Sporzynski A, Pispas S, Kovacik L, Stepanek M. Glucose-Responsive Hybrid Nanoassemblies in Aqueous Solutions: Ordered Phenylboronic Acid within Intermixed Poly(4-hydroxystyrene)-block-poly(ethylene oxide) Block Copolymer. Biomacromolecules. 2015; 16:3731–3739. [PubMed: 26509848]
43. Qiu FY, Zhang M, Ji R, Du FS, Li ZC. Oxidation-Responsive Polymer-Drug Conjugates with a Phenylboronic Ester Linker. Macromolecular rapid communications. 2015; 36:2012–2018. [PubMed: 26297612]
44. Zhu JY, Lei Q, Yang B, Jia HZ, Qiu WX, Wang X, Zeng X, Zhuo RX, Feng J, Zhang XZ. Efficient nuclear drug translocation and improved drug efficacy mediated by acidity-responsive boronate-linked dextran/cholesterol nanoassembly. Biomaterials. 2015; 52:281–290. [PubMed: 25818434]
45. Yang B, Lv Y, Zhu JY, Han YT, Jia HZ, Chen WH, Feng J, Zhang XZ, Zhuo RX. A pH-responsive drug nanovehicle constructed by reversible attachment of cholesterol to PEGylated poly(l-lysine) via catechol-boronic acid ester formation. Acta biomaterialia. 2014; 10:3686–3695. [PubMed: 24879311]
46. Yao Y, Zhao L, Yang J. Glucose-responsive vehicles containing phenylborate ester for controlled insulin release at neutral pH. Biomacromolecules. 2012; 13:1837–1844. [PubMed: 22537190]
47. Chen W, Cheng Y, Wang B. Dual-responsive boronate crosslinked micelles for targeted drug delivery. Angew Chem Int Ed Engl. 2012; 51:5293–5295. [PubMed: 22511250]
48. Springsteen G, Wang BH. A detailed examination of boronic acid-diol complexation. Tetrahedron. 2002; 58:5291–5300.

49. Desai N, Trieu V, Yao Z, Louie L, Ci S, Yang A, Tao C, De T, Beals B, Dykes D, Noker P, Yao R, Labao E, Hawkins M, Soon-Shiong P. Increased antitumor activity, intratumor paclitaxel concentrations, and endothelial cell transport of cremophor-free, albumin-bound paclitaxel, ABI-007, compared with cremophor-based paclitaxel. Clinical cancer research : an official journal of the American Association for Cancer Research. 2006; 12:1317–1324. [PubMed: 16489089]
50. Jares-Erijman EA, Jovin TM. FRET imaging. Nat Biotechnol. 2003; 21:1387–1395. [PubMed: 14595367]
51. Sapsford KE, Berti L, Medintz IL. Materials for fluorescence resonance energy transfer analysis: beyond traditional donor-acceptor combinations. Angew Chem Int Ed Engl. 2006; 45:4562–4589. [PubMed: 16819760]
52. Morton SW, Zhao X, Quadir MA, Hammond PT. FRET-enabled biological characterization of polymeric micelles. Biomaterials. 2014; 35:3489–3496. [PubMed: 24477190]
53. Kim KS, Kim JH, Kim H, Laquai F, Arifin E, Lee JK, Yoo SI, Sohn BH. Switching off FRET in the hybrid assemblies of diblock copolymer micelles, quantum dots, and dyes by plasmonic nanoparticles. ACS nano. 2012; 6:5051–5059. [PubMed: 22621410]
54. Xiao K, Li Y, Luo J, Lee JS, Xiao W, Gonik AM, Agarwal RG, Lam KS. The effect of surface charge on in vivo biodistribution of PEG-oligocholic acid based micellar nanoparticles. Biomaterials. 2011; 32:3435–3446. [PubMed: 21295849]
55. Dittrich C, Kosty M, Jezdic S, Pyle D, Berardi R, Bergh J, El-Saghir N, Lotz JP, Osterlund P, Pavlidis N, Purkalne G, Awada A, Banerjee S, Bhatia S, Bogaerts J, Buckner J, Cardoso F, Casali P, Chu E, Close JL, Coiffier B, Connolly R, Coupland S, De Petris L, De Santis M, de Vries EG, Dizon DS, Duff J, Duska LR, Eniu A, Ernstoff M, Felip E, Fey MF, Gilbert J, Girard N, Glaudemans AW, Gopalan PK, Grothey A, Hahn SM, Hanna D, Herold C, Herrstedt J, Homicsko K, Jones DV Jr, Jost L, Keilholz U, Khan S, Kiss A, Kohne CH, Kunstfeld R, Lenz HJ, Lichtman S, Licitra L, Lion T, Litiere S, Liu L, Loehrer PJ, Markham MJ, Markman B, Mayerhoefer M, Meran JG, Michielin O, Moser EC, Mountzios G, Moynihan T, Nielsen T, Ohe Y, Oberg K, Palumbo A, Peccatori FA, Pfeilstocker M, Raut C, Remick SC, Robson M, Rutkowski P, Salgado R, Schapira L, Schernhammer E, Schlumberger M, Schmoll HJ, Schnipper L, Sessa C, Shapiro CL, Steele J, Sternberg CN, Stiefel F, Strasser F, Stupp R, Sullivan R, Tabernero J, Travado L, Verheij M, Voest E, Vokes E, Von Roenn J, Weber JS, Wildiers H, Yarden Y. ESMO/ASCO Recommendations for a Global Curriculum in Medical Oncology Edition 2016. ESMO open. 2016; 1:e000097. [PubMed: 27843641]
56. Ren Y, Jiang R, Yin S, You C, Liu D, Cheng X, Tang J, Zang R. Radical surgery versus standard surgery for primary cytoreduction of bulky stage IIIC and IV ovarian cancer: an observational study. BMC cancer. 2015; 15:583. [PubMed: 26268818]
57. Bristow RE, Chang J, Ziogas A, Anton-Culver H, Vieira VM. Spatial analysis of adherence to treatment guidelines for advanced-stage ovarian cancer and the impact of race and socioeconomic status. Gynecologic oncology. 2014; 134:60–67. [PubMed: 24680770]

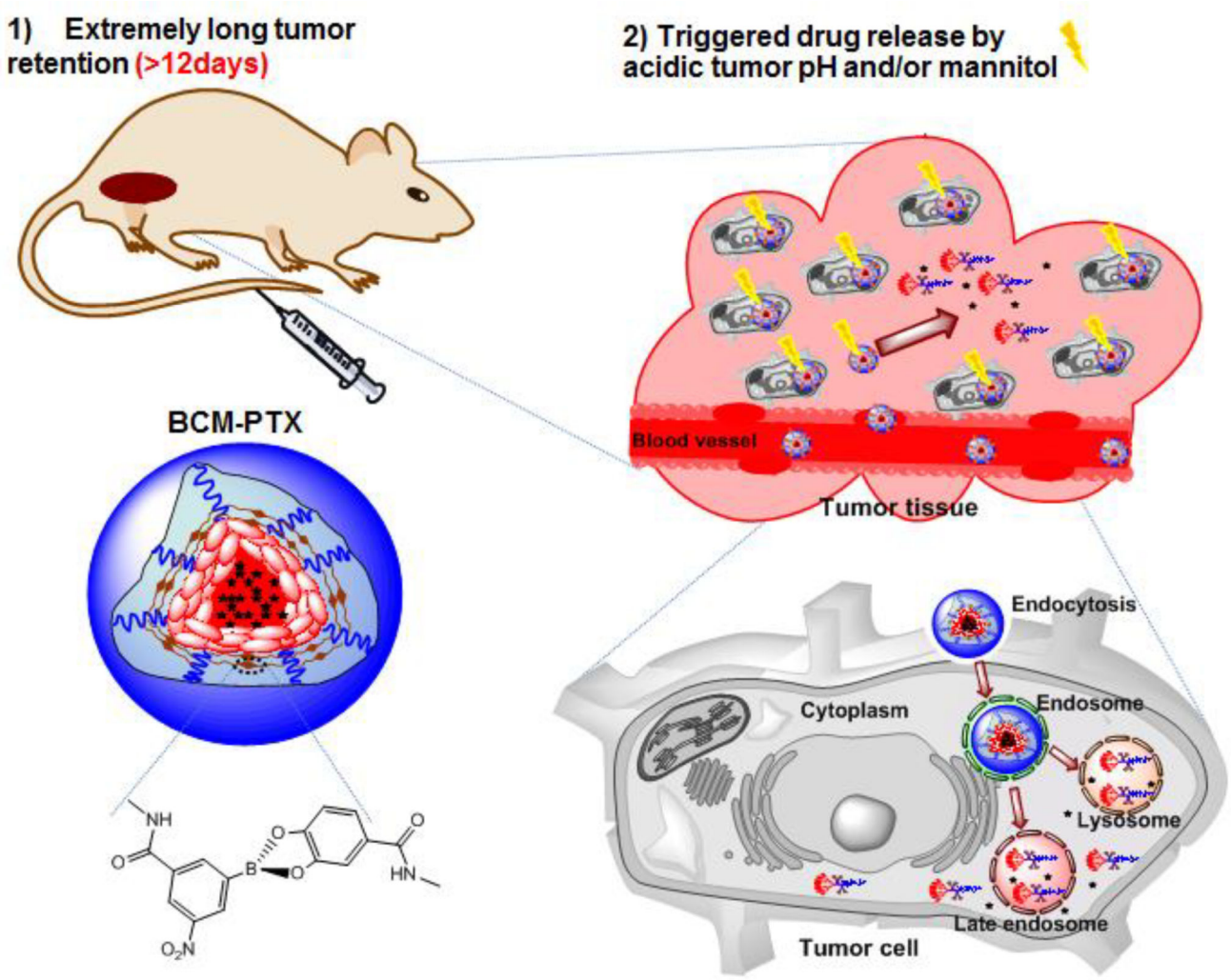

Figure 1.

Schematic illustration of long tumor retention, dual-sensitive boronate cross-linked micelles (BCM) for cancer therapy.

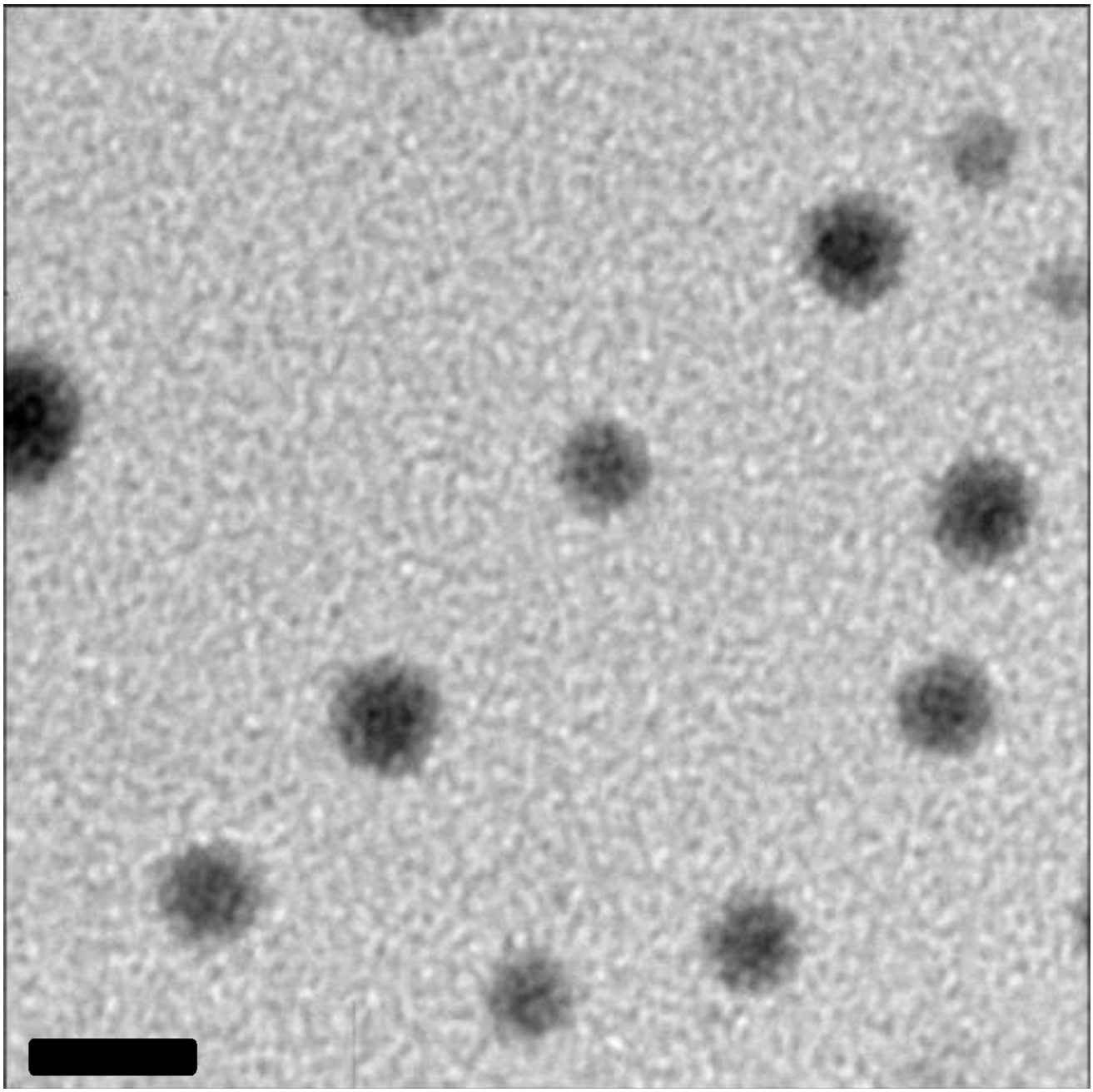

Figure2.
TEM images of PTX loaded BCM in PBS. (PTX loading was 2.0 mg/mL, TEM scale bar: 50 nm)

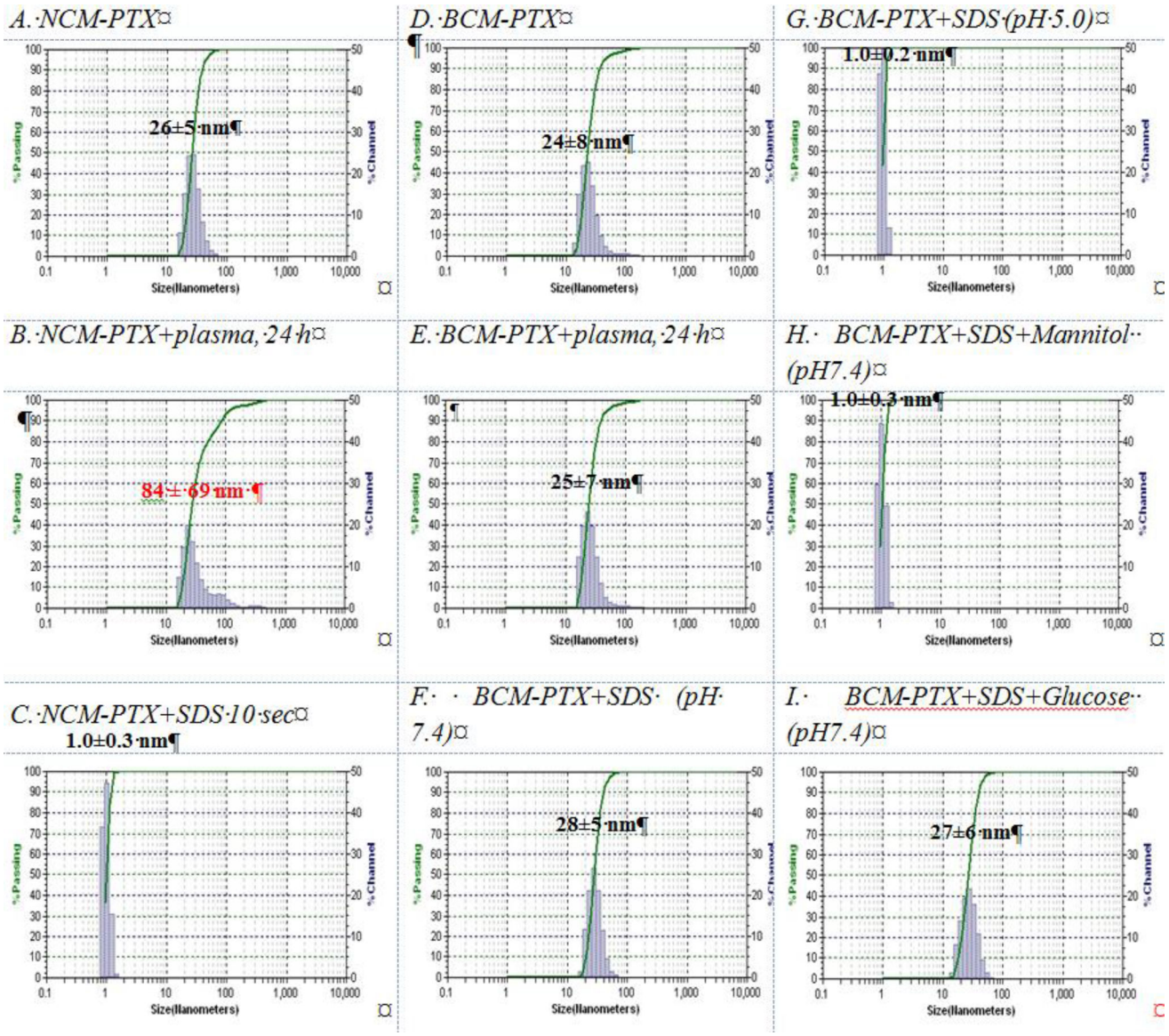

Figure 3.

The particle size of paclitaxel loaded non-crosslinked micelles (NCM-PTX) in the absence (**A**) and in the presence (**B**) of plasma 50% (v/v) for 24 h; The particle size of NCM-PTX in the presence of 2.5 mg/mL SDS for 10 sec (**C**);The particle size of boronate crosslinked micelles (BCM-PTX) in the absence (**D**) and in the presence of plasma 50% (v/v) for 24 h (**E**);The particle size of BCM-PTX in the presence of 2.5 mg/mL SDS for 120 min (**F**);The particle size of BCM-PTX in SDS for 120 min and then adjusted the pH of the solution to 5.0 for 20 min (**G**); The particle size of BCM-PTX in SDS for 120 min and then treated with mannitol (100 mM) for 20 min (**H**); The particle size of BCM-PTX in SDS for 120 min and then treated with glucose (100 mM) for 20 min. The particle size was measured by DLS (Microtrac).The concentration of micelles was kept at 1.0 mg/mL in PBS.

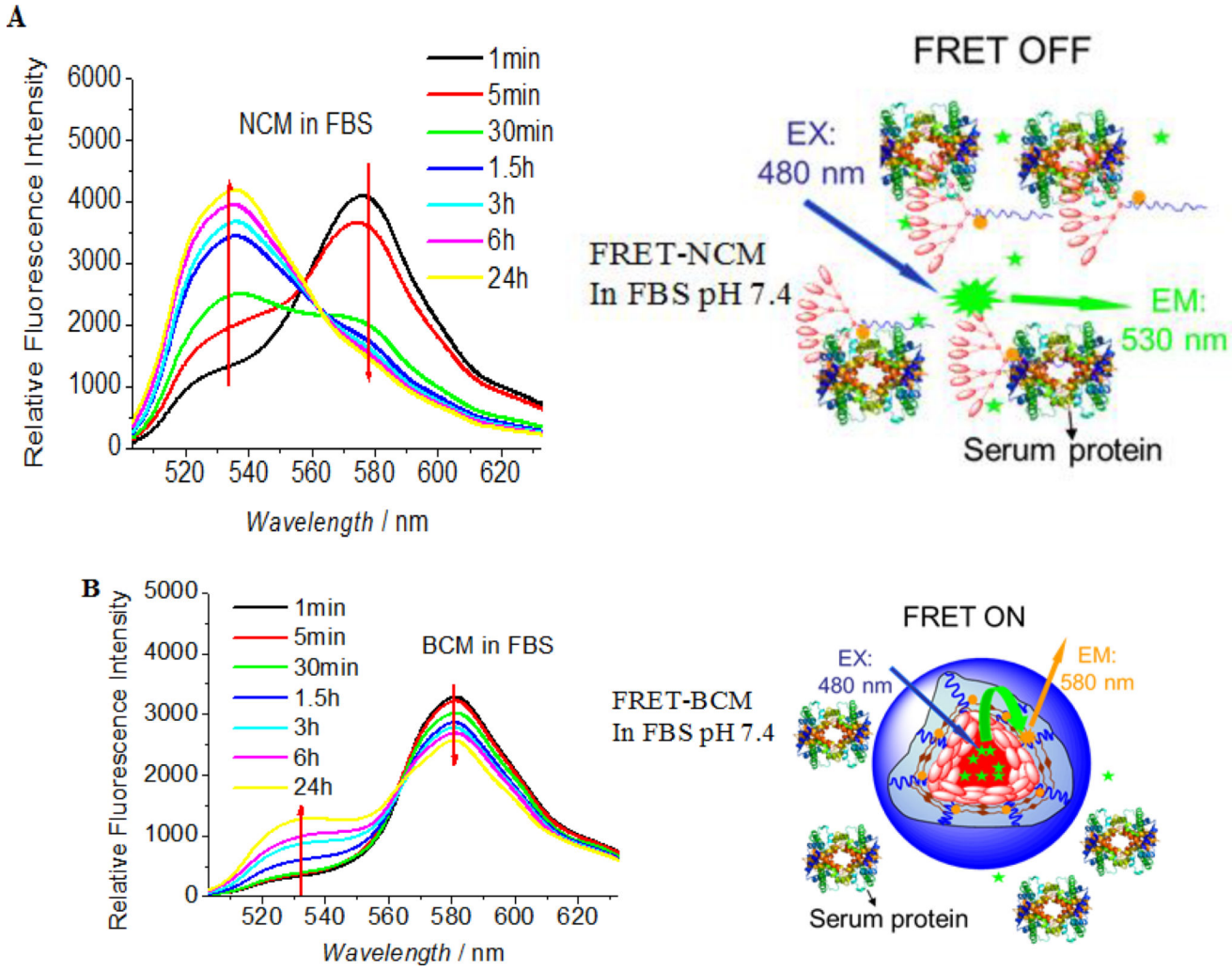

Figure 4.

Fluorescence spectra and schematic illustration of (**A**) non-crosslinked FRET micelles (NCM) and (**B**) boronate crosslinked FRET micelles (BCM) in FBS, respectively. The concentration of the micelles was 0.1 mg/mL. Excitation: 480 nm.

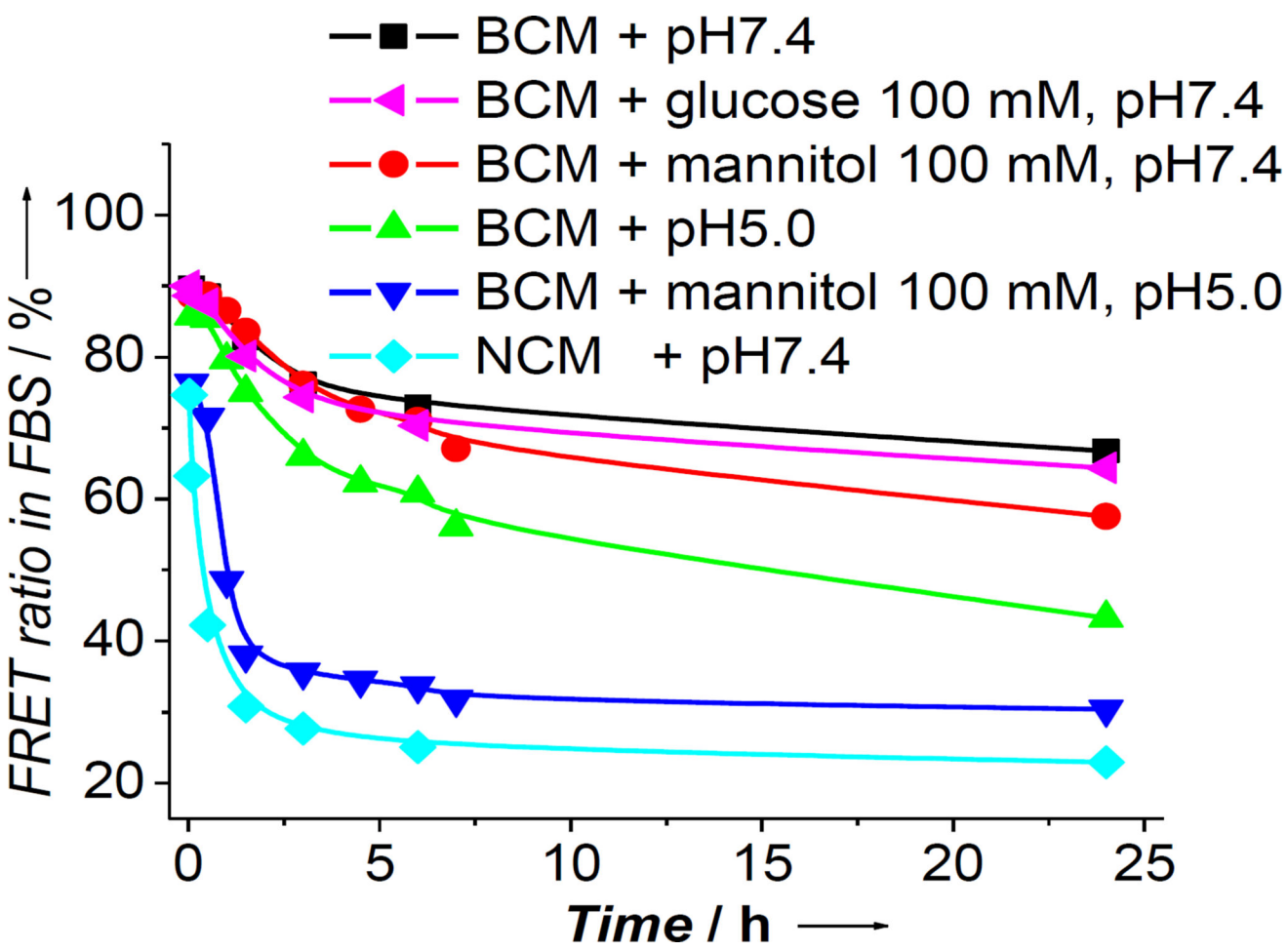

Figure 5.

The changes in FRET ratio of FRET-BCM in FBS at different pH values and in the presence of sugars compared with that of FRET-NCM in FBS at pH7.4. The final concentration of the micelles was 0.1 mg/mL. Excitation: 480 nm.

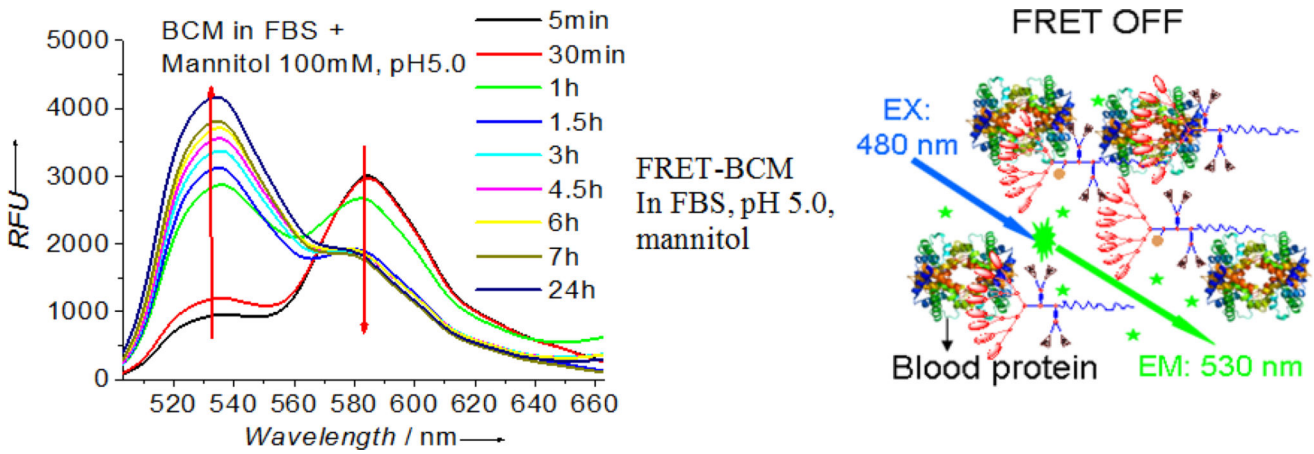

Figure 6.

Fluorescence spectra and schematic illustration of FRET-BCM in FBS at pH5.0 in the presence of mannitol (100mM) over time. The final concentration of the micelles was 0.1 mg/mL. Excitation: 480 nm.

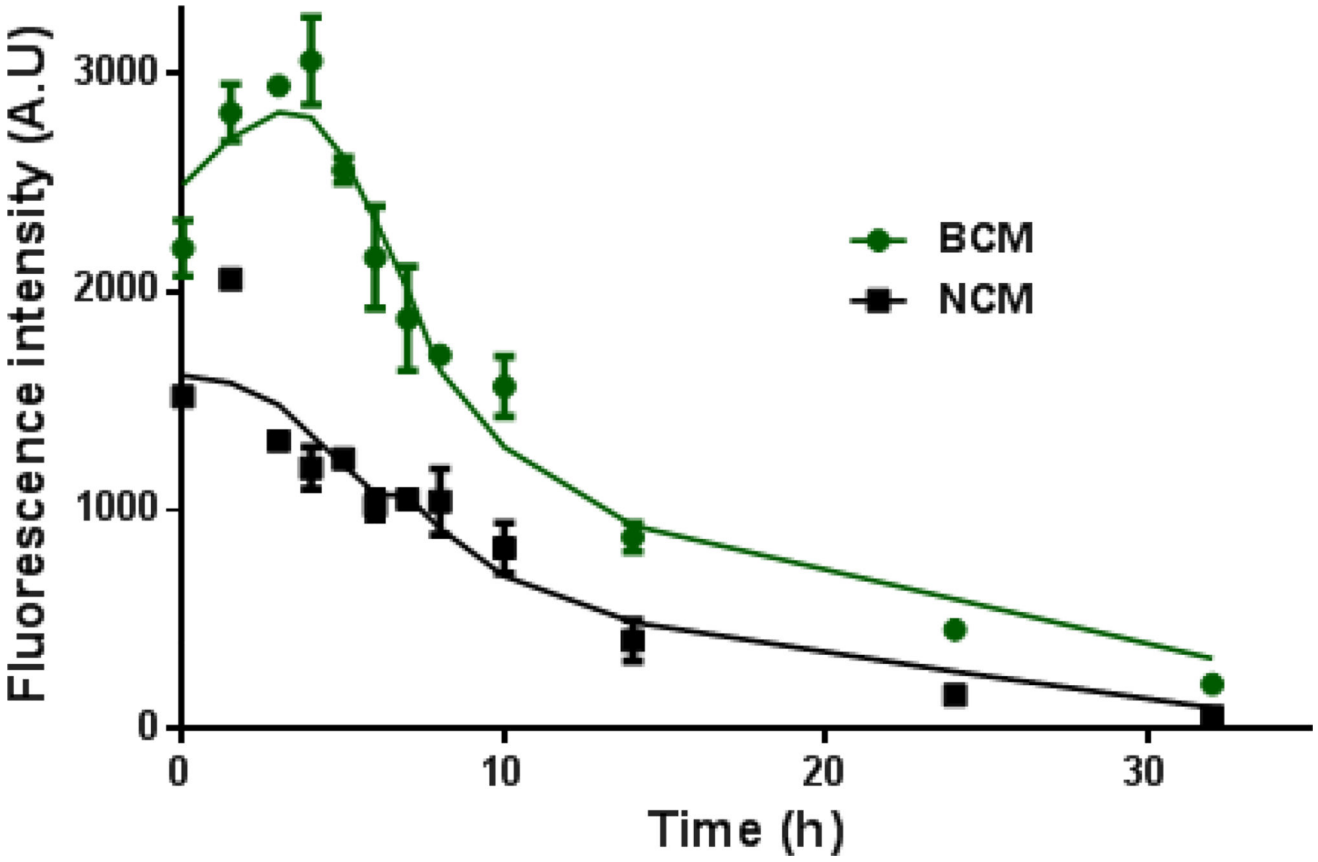

Figure 7.

In vivo blood elimination of DiD-loaded BCM and NCM in nude mice bearing SKOV-3 ovarian cancer xenograft (DiD: 0.5 mg/mL, 100 μL injection volume) (n=3).

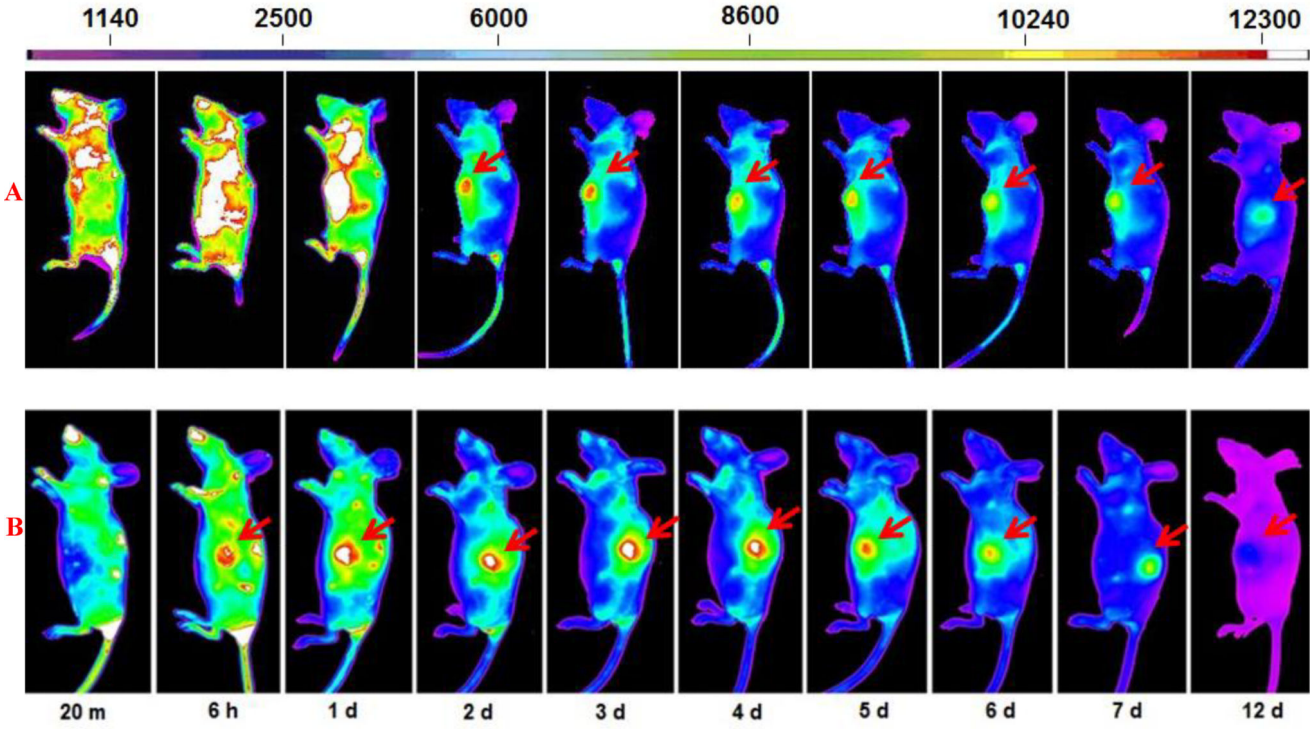

Figure 8.

The *in vivo* NIRF imaging of nude mice bearing SKOV3 xenografts after injection of DiD loaded BCM (A) and NCM (B). Mice were given 100 μL DiD and PTX co- loaded BCM or NCM (0.5 mg/mL of DiD; 0.5 mg/mL of PTX) via tail vein and NIRF imaging was acquired at 20 min, 6hrs, 1, 2, 3, 4, 5, 6, 7 and 12 days post-injection. Red arrows: SKOV3 tumors. N=3, representative results reported.

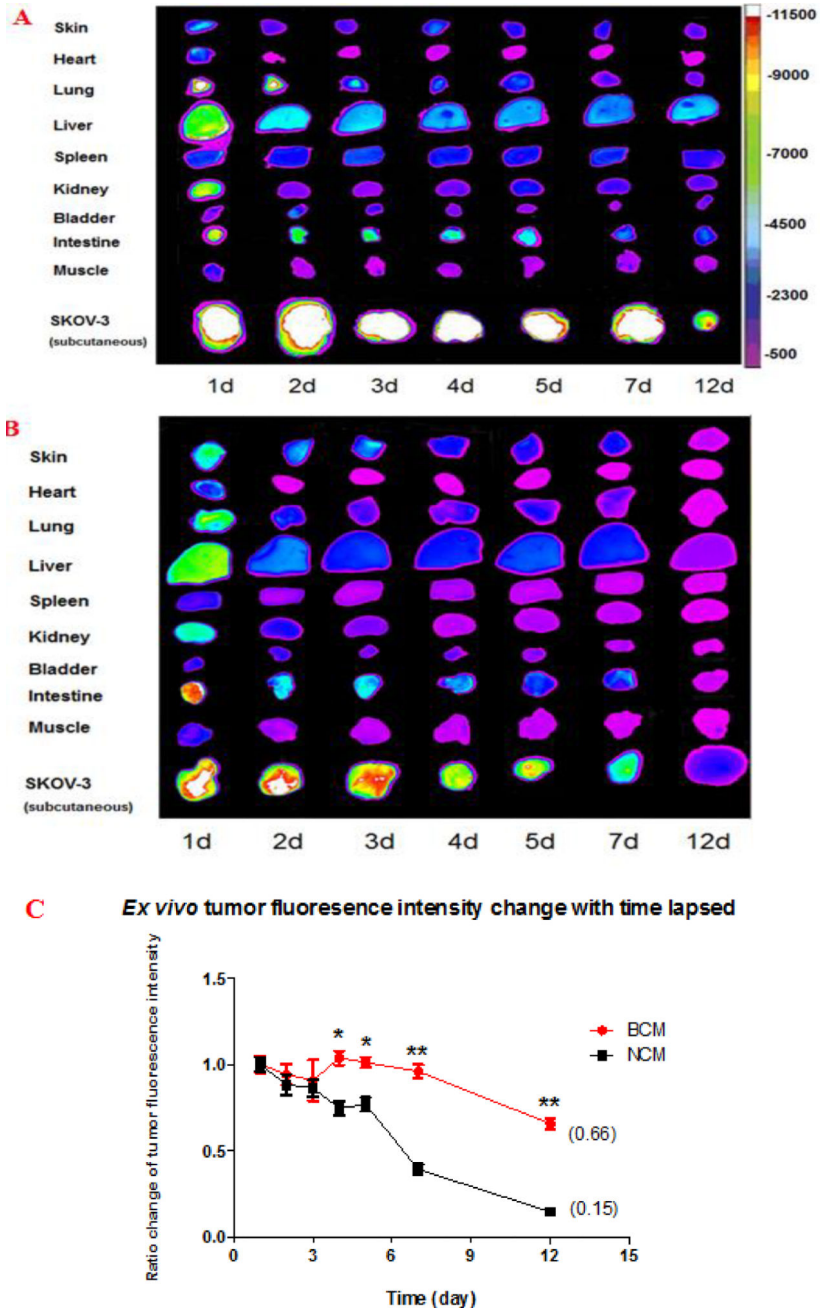

Figure 9.

The ex vivo NIRF imaging of tumors and major organs of nude mice bearing SKOV3 xenografts up to 12 days post-injection of DiD and PTX co-loaded BCM (A) or NCM (B) and the tumor fluorescence intensity changes (C). Mice were given 100 μL DiD and PTX co-loaded BCM or NCM (0.5 mg/mL of DiD; 0.5 mg/mL of PTX) via tail vein and *ex vivo* NIRF imaging was acquired at 1, 2, 3, 4, 5, 6, 7 and 12 days post-injection. Red arrows: SKOV3 tumors. * : $p<0.05$, **: $P<0.01$. N=3, representative results reported.

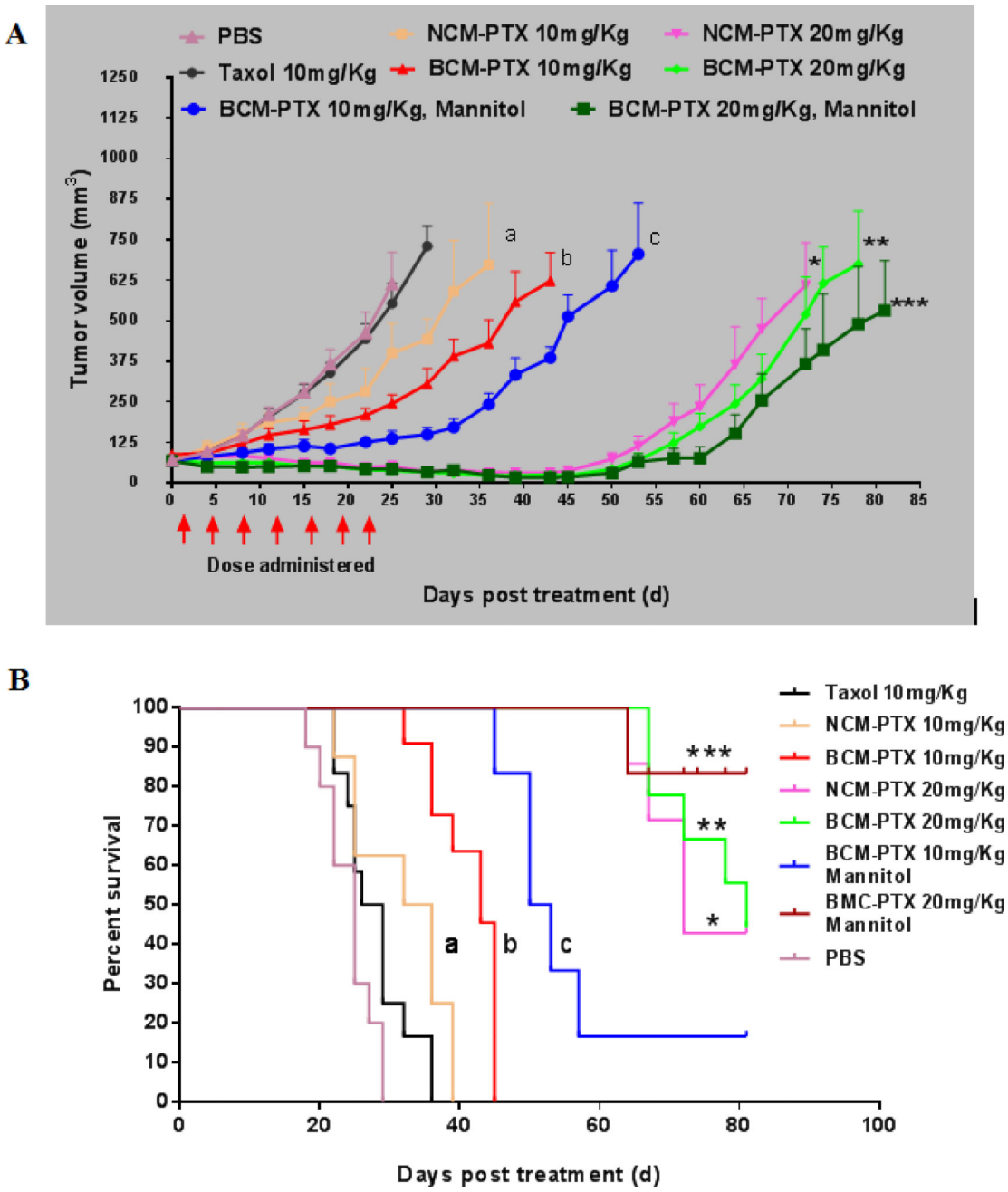

Figure 10.

Tumor volume change (**A**) and survival curve (**B**) of nude mice bearing SKOV-3 xenografts treated with various formulations of paclitaxel, non-cross- linked and boronate-catechol cross- inked nanoparticles, with and without mannitol given 24 hrs after each dose of nanoparticle drug. Arrows: treatments. Tumor volume (Mean ± SEM). a, b and c are significantly different from each other, $p<0.05$. *, ** and *** are significantly different from each other, $p<0.05$.

Table 1

The particle size of paclitaxel loaded non-crosslinked micelles (NCM-PTX) and boronate crosslinked micelles (BCM-PTX) under various conditions.

	PBS	plasma, 24 h	SDS (pH 7.4)	SDS (pH 5.0)	SDS+Mannitol (pH7.4)	*SDS+Glucose (pH7.4)*
NCM-PTX	26±5 nm	84 ± 69 nm	1.0±0.3 nm			
BCM-PTX	24±8 nm	25±7 nm	28±5 nm	1.0±0.2 nm	1.0±0.3 nm	27±6 nm